ORIGINAL ARTICLE

Characterisation of defects in porous silicon as an anode material using positron annihilation Doppler Broadening Spectroscopy

W. J. Legerstee[1,2] · T. Noort[1] · T. K. van Vliet[2] · H. Schut[3] · E. M. Kelder[1]

Abstract

Here we present Positron Annihilation Doppler Broadening Spectroscopy (PADBS) as a powerful method to analyse the origin and development of defect processes in porous silicon structures as a result of alloying with lithium for the use in battery anode applications. Several prepared anodes were lithiated (discharged against Li$^+$/Li) and de-lithiated (charged) with different capacities followed by a distinct treatment procedure and an analysis using the Delft Variable Energy Positron Beam. The results presented here show that we can distinguish two different processes attributed to (1) structural changes in silicon as a result of the alloying process, and (2) the formation of defects that initiate degradation of the material. The limit at which the porous material can be used for at least the first two cycles without the occurrence of damage can thus be accurately determined by using the PADBS technique.

Keywords Silicon lithium alloy · Silicon anode · Positron annihilation · Porous silicon

Introduction

The automotive industry needs higher energy densities for lithium ion batteries. To achieve this, a great deal of research is being conducted into new materials, including anode materials. Silicon is seen as the next-generation anode material in Li-ion batteries because its theoretical capacity of 3579 mAh g^{-1} (based on Li$_{15}$Si$_4$) is up to more than ten times higher than the commonly used graphite anodes with a theoretical capacity of approx. 372 mAh g^{-1} (Li and Dahn 2007; Liu and Huang 2011). However, silicon's ability to alloy with lithium results in a large volume expansion up to 300–400 percent. The mechanical stresses created by volume expansion cause cracking and particle pulverization, resulting in electrically disconnected small particles and poor contact with the current collector, followed by capacitance loss and anode degradation (Beaulieu et al. 2001). To overcome these major drawbacks, several research groups have sought ways to accommodate these extreme volume changes. One of the possible solutions is the incorporation of small open volumes, e.g. voids, in silicon structures at which a large part of the volume increase can be absorbed thus preventing the formation of cracks in the silicon anode material (McDowell et al. 2013; Shen et al. 2016; Shin et al. 2005), as illustrated schematically in Fig. 1.

In the past decade, various structural material designs containing open volumes have been developed, among which silicon-carbon composites (Kim et al. 2018), silicon nanowires (Zamfir et al. 2013; Salihoglu and Kahlout 2019) hollow nano structures (Yeom et al. 2019; Wang et al. 2018), and nano structured layers (Tang et al. 2019; Cho 2010). However, many of these methods have the significant drawback of being based on advanced deposition techniques capable of producing only small amounts of material, making it unsuitable for use in the automotive industry where large-scale electrode material production is required. Therefore, many research groups have focused on scalable methods for the production of micro-sized particles containing nano-sized porosity (Wang et al. 2020; An

✉ W. J. Legerstee
w.j.legerstee@tudelft.nl

1 Department Storage of Electrochemical Energy, Reactor Institute Delft, Delft University of Technology, Mekelweg 15, 2629 JB Delft, The Netherlands

2 Department Automotive, Institute for Engineering and Applied Sciences, Rotterdam University of Applied Sciences, Heijplaatstraat 23, 3089 JB Rotterdam, The Netherlands

3 Department Radiation Science and Technology, Delft University of Technology, Mekelweg 15, 2629 JB Delft, The Netherlands

Fig. 1 The principle of absorbing expansion due to silicon lithiation by structures containing small open volumes
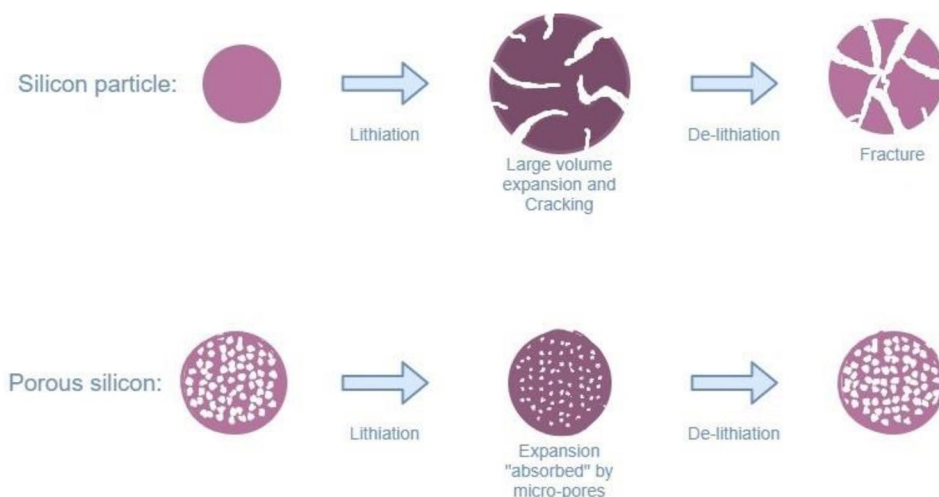
et al. 2019; Ge et al. 2013; Zhang et al. 2014) which can be processed into battery electrodes using the well-known tape-casting methods (Shanefield 1991).

However, the use of porous materials in commercial batteries requires insight into the limitations due to the degradation processes caused by charging and discharging the anode material repeatedly (cycling). In addition to the more usual analysis methods, like long-term cycling tests, electro-chemical impedance analysis, intermittent titration techniques and cyclic voltametric analysis, researchers use various advanced analysis methods, including Transmission Electron Microscopy (Shen et al. 2016; McDowell et al. 2012), acoustic emission (Kalnaus et al. 2011; Rhodes et al. 2010), Atomic Force Microscopy (Vidu et al. 2002; Huang et al. 2018) and Nuclear Magnetic Resonance (Key et al. 2011). More recently, methods such as X-ray Compton scattering spectroscopy (Suzuki et al. 2016) and positron annihilation spectroscopy (Klinser et al. 2019; Seidlmayer et al. 2016) have been used to investigate the presence and change of defects as a result of lithium extraction and uptake in cathode electrode materials. Here we present Positron Annihilation Doppler Broadening Spectroscopy (PADBS) as a new additional powerful technique for the defect characterization of silicon anodes. Due to its high sensitivity to open volume defects (Krause-Rehberg and Leipner 1999), we have applied this technique for the study of early stage crack formation. The value of this method is demonstrated on porous silicon anodes by determining a critical charging capacity above which the defect structure is changing. The change in PADBS parameters is related to premature fracture of the porous particles caused by the expansion of the silicon as a result of the alloying process with lithium. For this study, we use porous silicon that has been successfully and scalable produced and which is available as a bulk material for anode preparation (E-magy 2020).

Experimental

Positron annihilation Doppler broadening spectroscopy

Positron Annihilation Spectroscopy (PAS) is a well-established nondestructive technique for characterization of defects, voids and open volumes in materials (Schultz and Lynn 1988), and is used in many fields of material science (Tyomisto and Makkonen 2013). The use of positron annihilation as a probe allows for the detection of defect concentrations of the order of 0.1 ppm (Smedskjaer et al. 1980) which makes this technique extremely sensitive. Several positron measurement principles are known (Krause-Rehberg and Leipner 1999) and used for almost 50 years to characterize defects in materials. The method we use here is the so-called Variable Energy Positron beam Doppler Broadening technique, which measures the Doppler shift in the energy of the 511 keV annihilation gammas emitted when a positron annihilates.

Positrons are anti-matter particles and can be created by materialization of radiation (e^+/e^- pair production) or are obtained by β^+ decay. For the latter usually a ^{22}Na positron source is used which emits positrons with kinetic energies distributed according to a so-called beta-spectrum. To obtain a beam of positrons with tunable, well defined energies the positrons emitted by the ^{22}Na source are slowed down to an energy of ~2.5 eV by using a Tungsten moderator. These moderated positrons are then accelerated to selected energies (practically between 0.1 and 25 keV) and targeted on a material of interest. When implanted in a sample with an initial kinetic energy well above the thermal energy, the positrons rapidly lose their energy. When thermal equilibrium is reached, positron–electron annihilation can take place, most likely resulting in the

collinear emission of two 511 keV photons. Due to the momentum of the positron–electron pair (mainly determined by the electron motion) the photon energies show a Doppler shift which causes a broadening of the annihilation energy distribution when observed by an energy selective spectrometer. The shape of the obtained energy spectrum is related to the presence and type of defects and is commonly characterized by the so-called shape parameters S and W, as shown in Fig. 2ᵃ. The S parameter is experimentally determined as the relative area of the central part of the energy distribution spectrum, while the W parameter expresses the relative contributions of the tails to the total peak area (Clement et al. 1996). Thus, the S parameter is a measure for the contribution of lower momentum (valance) electrons, while the W parameter represents annihilations with the higher momentum (core) electrons. By determining these parameters for a series of implantation energies (related to depth), defect depth distributions and characterization of open volume defects in sub-surface regions can be obtained. The defect S parameter is most sensitive to defects because the probability for a positron to annihilate with high momentum outer shell electrons of defect neighboring atoms is lower, thus increasing the contribution of low momentum annihilations in the 511 keV photo-peak.

The variable energy positron beam

For Positron Annihilation Doppler Broadening Spectroscopy (PADBS) measurements, we used the Delft Variable Energy Positron Beam (VEP), containing a ^{22}Na positron source (1 GBq) to produce a mono-energetic, magnetically guided positron beam (~ 105 e + .s^{-1}) with a diameter of 8 mm and variable acceleration energy ranging from 1 to 25 keV for depth selective probing. The corresponding depth range can be determined from the following power law (Schurtz and Lynn 1988):

$$\bar{z} = \frac{A}{\rho} E^n$$

where $\bar{z}$ is the mean implantation depth (in Å), ρ is the density of the target material (2.3 g cm^{-3} for Si), A is a constant empirically found to be $A \approx 400$ Å g cm^3 keV^{-n} and $n \approx 1.6$ for most materials (Lynn and Lutz 1980). The maximum average implantation depth can be determined for silicon at approximately 3µ for 25 keV positrons. Energy selective measurements of the annihilation radiation are performed with a high purity Ge solid state detector (Canberra, energy resolution 1.8 keV@1.33 MeV) in single-detector mode (as shown schematically in Fig. 2b). For analysis of the obtained S and W parameter, the data fitting and modeling algorithm VEPFIT is used (Van Veen et al. 1991).

Lithiation of porous silicon

The electro-chemical lithiation process of crystalline silicon (c-Si) is a two phase alloying process with a sharp reaction front (Chon et al. 2011; Obrovac and Christensen 2004). During the first lithiation c-Si is transformed to an amorphous Li$_x$Si alloy ($0 < x < 3.4$) forming a distinct voltage plateau in the potential curve (first discharge part in Fig. 5) around 0.1 V versus Li$^+$/Li (indicating the two phase addition reaction between Si and Lithium), and with a volume change of $\sim 300\%$ (for $x = 3.4$). Further (or deep) lithiation to a voltage under ~ 0.05 V will form a crystalline and metastable Li$_{15}$Si$_4$ alloy which is the final lithiated product for electro-chemical alloying at room temperature (Obrovac and Christensen 2004; Kubota et al. 2007). In de-alloying (extract lithium), the crystalline structure (Li$_{15}$Si$_{4)}$ will revert to amorphous Li$_y$Si ($y \approx 2$) by a two phase reaction at a distinct plateau at ~ 0.4 V, followed by a solid-solution reaction from amorphous Li$_y$Si to amorphous silicon (a-Si) when completely de-lithiated (Zhang 2011). The second and subsequent alloying and de-alloying cycles show up a voltage profile which is different from the first, as can be seen
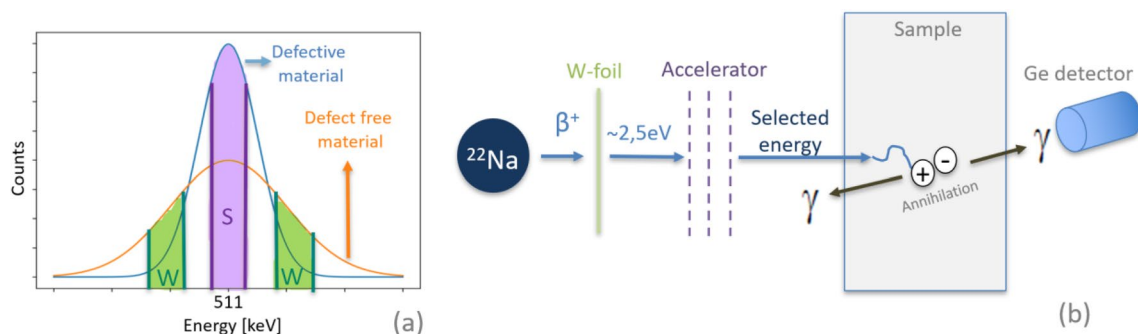

Fig. 2 **a** Energy distribution spectra of a defect-free sample (orange) and a defective material (blue), and the shape parameters S (purple) and W (green). **b** PADBS measurement principle for single-detector mode in which one out of the two Gamma rays is detected

in Fig. 5. For better cycling performance, it is recommended to avoid the forming of the crystallized $Li_{15}Si_4$ phase by setting the lower voltage limit on 50 mV. (Li and Dahn 2007; Ozanam and Rosso 2016).

The shape of the voltage profiles for Si-anodes is affected, among other things, by the morphological properties of the used silicon material. Anodes that contain silicon with different porosity structure or particle size show up slightly different voltage profiles (different slopes of the curves) because alloying processes are highly influenced by the ratio between surface/interface processes and particle volume (Zhang 2011). In Fig. 5 the voltage profile of the material used for this study is shown.

Several studies have indicated that particularly during the very first lithiation, extensive damage occurs in the c-Si structure (Kalnaus et al. 2011; McDowell et al. 2013). With porous Si structures, the occurrence of damage is partly determined by the ability of the open volumes to absorb the expansion. Thus for using these materials in commercial batteries, it is important to know the limit of lithiation before cracking occurs. This means, the theoretical capacity of 3579 mAh g^{-1} will not be fully used, but instead the maximum capacity without fracture (C_{max}) will be the desired value at which the anode material can be used with minimal degradation over longer time. For porous silicon, C_{max} is

determined by the ability of the porosities to compensate for volume changes due to lithiation. In Fig. 3 a simplified pore-compensation mechanism is schematically shown wherein the occurring volume change due to alloying ($\Delta V_{alloying}$) is compared with the compensating pore volume (V_{pores}). The first situation when $\Delta V_{alloying} < V_{pores}$ will prevent for damage because the discharged capacity (C_d) is below C_{max}. The second situation is the equilibrium state where $\Delta V_{alloying} = V_{pores}$ where C_d will be equal to C_{max}, that is the status we want to approach as closely as possible. In the third situation, $\Delta V_{alloying} > V_{pores}$, the value of C_d exceeds C_{max} resulting that some of the expansion will cause fractures and permanent damage will occur. Determining the critical value of C_{max} is for commercial use of porous silicon very valuable because in addition to preventing damage, the capacity to be used can be accurately determined so that the material can be used optimally.

Atomic force microscopy analysis

The absorption of expansion by the porous Si as a result of lithium alloying is analyzed with an Atomic Force Microscope (AFM) (Ntegra NT-NDT) which is located in a glovebox under inert atmosphere (Legerstee et al. 2021). An open cell design allows the AFM probe (Pointprobe

Fig. 3 Schematic represenatation of volume expansion compensation and limits by porous silicon
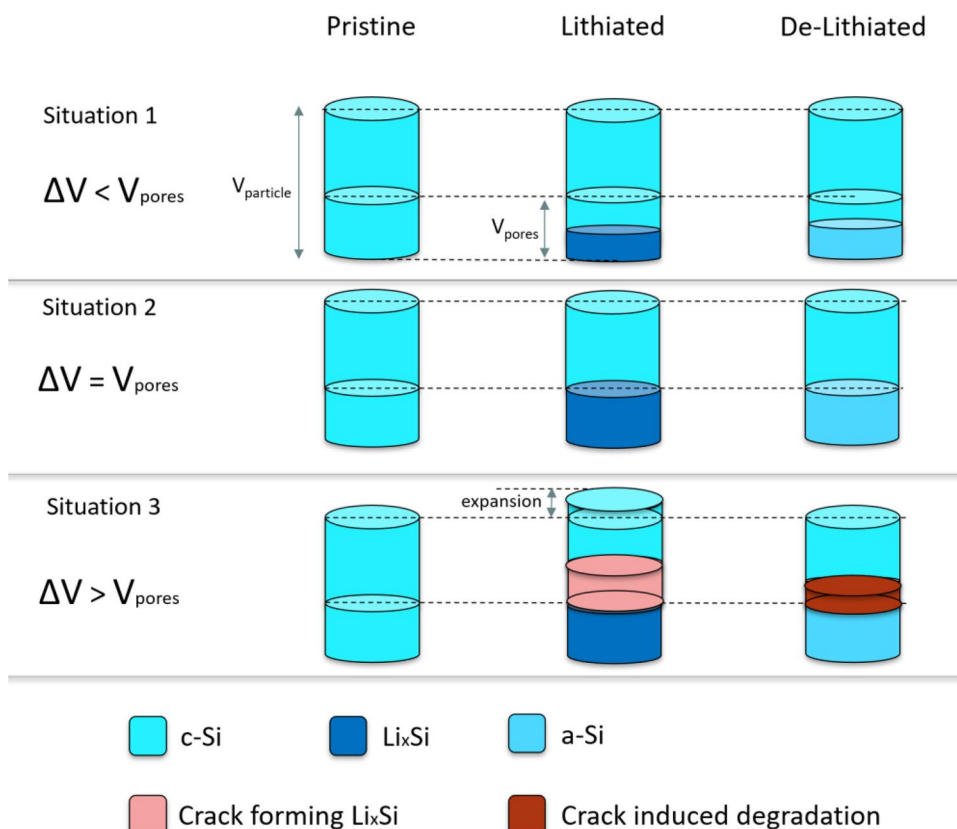
Fig. 4 **a** SEM picture of flake surface, **b** XRD patern c-Si flake, **c** SEM picture of prepared anode (80 m% porous Si), **d** SEM detail of a porous particle
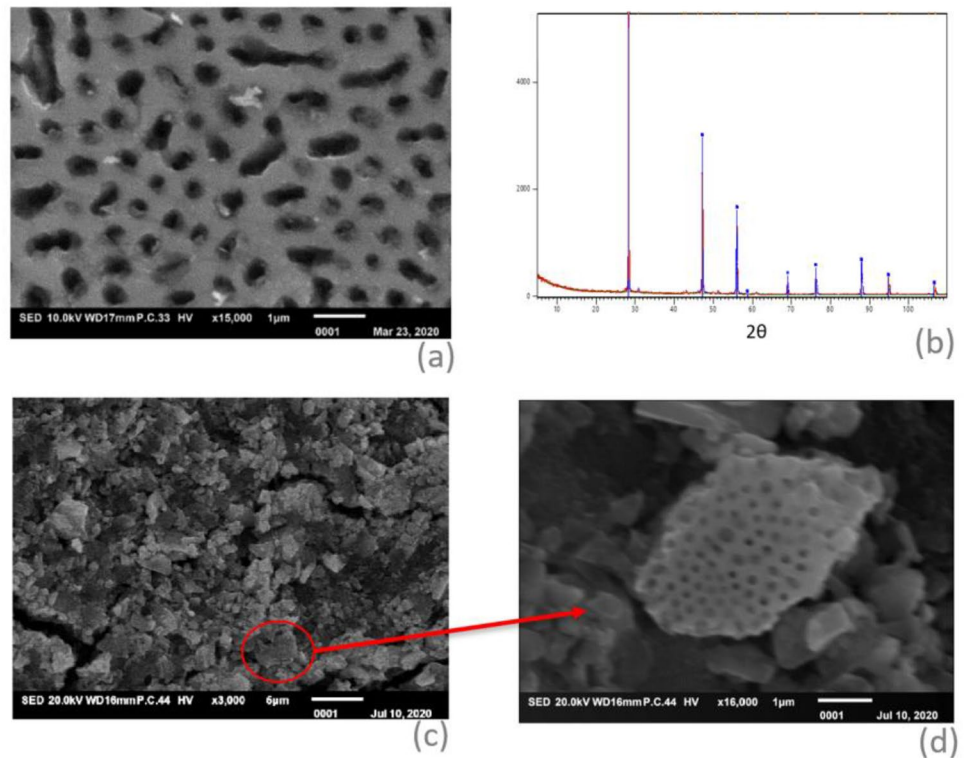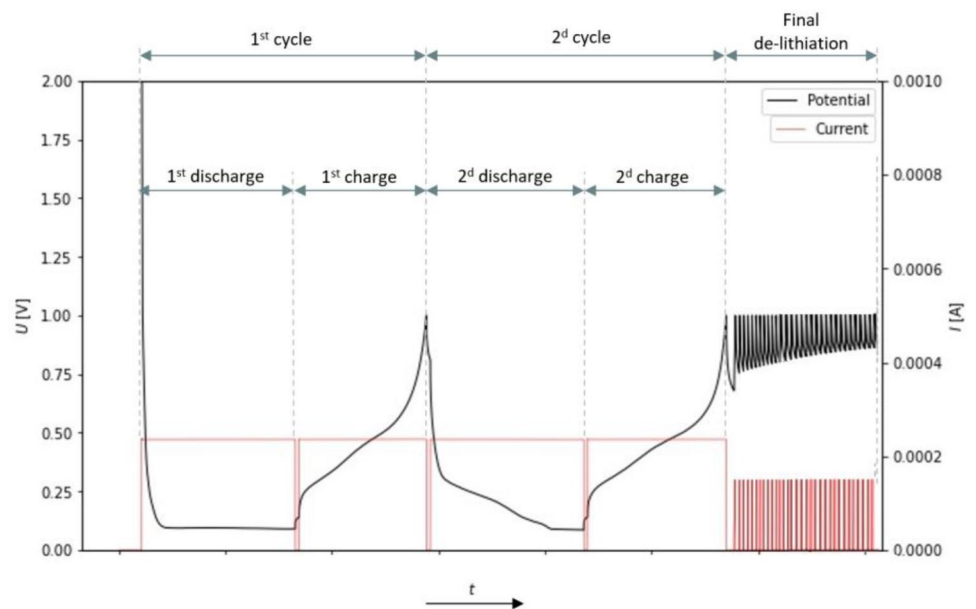

Fig. 5 Cylcling procedure of porous silicon anode samples in a half-cell configuration (metallic lithium as a counter and reference electrode)

CDT-NCHR) to access the surface of a flake. After a scan it is possible to add electrolyte and lithiate the flake surface, after which the surface can be carefully cleaned of the electrolyte and a new scan of the surface can be made.

Sample preparation

Porous c-Si was obtained from E-magy in two different appearances, as half product (so-called 'flakes') and in the

form of 2–6 μm sized particles. The flakes are used for additional surface analysis by Scanning Electron Microscopy (SEM) (JEOL JSM-IT100) and AFM, while the particles are used to prepare electrodes by a doctor blade casting method. Figure 4a shows a SEM photo of the base material (flake). Due to the pores of the material (200–600 nm), a porosity of approximately 35% is obtained (according to the specs of the supplier). The XRD pattern of the porous c-Si confirms the presence of a crystalline phase (Fig. 4b).

Electrodes were prepared by mixing 80% porous Silicon particles with 10% Carbon Black, 10% Polyacrylic Acid (PAA) in a buffered critic acid solution was added to make a slurry. The slurry was coated on copper foil which acts as current collector for the prepared electrode and dried in a vacuum oven (60 °C for 12 h). Figure 4c, d shows a SEM picture of the prepared electrode and a detail of a porous particle. The anode sheets were cut into disks (diameter 12.7 mm) and assembled in an argon filled glovebox as a half-cell with lithium metal as a counter and reference electrode. To avoid the release of the anode material when dismounting the cells after cycling, we used a glass fiber membrane on the lithium metal side as a separator and polypropylene membrane (Cellgard 2400) on the silicon side, the former ensuring a stable amount of electrolyte. A dismountable laboratory cell (airtight mounted stainless steel poles separated by a PTFE gasket) was used to prepare the batteries with 1 M solution of $LiPF_6$ in 1:1 (vol%) ethylene carbonate (EC):dimethyl carbonate (DMC) as electrolyte. The samples were lithiated (discharged against Li^+/Li) and de-lithiated (charged) with c-rates based on $1C = 1000$mAh. g^{-1}, that is the capacity at which the porous material has been extensively tested and still shows capacity retention after 100 cycles (specified by the manufacturer).

Electro-chemical tests were carried out using a Maccor™ battery tester, and conducted under constant current conditions with a lower voltage limit on 0.05 V for preventing the formation of the unwanted crystalline $Li_{15}Si_4$ phase. The upper limit was set on 1 V for de-lithiation. We performed ten measurements with different values for C_d variating between 50 and 3000 mAh g^{-1}.The samples were cycled for 2 times at a current of 0.1C followed by a final de-lithiation step. In Fig. 5, an example of the cycling procedure is given. Here, the first cycle is the so-called 'Format step', followed by a full second cycling step. The last part, the final de-lithiation step, is added to attract as much as possible the lithium by charging (de-alloying) the sample repeatedly under a constant voltage of 1 V against Li^+/Li.

After the discharge/charge procedures the samples were prepared for PADBS measurements. The cells were dismounted in an airtight glovebox filled with argon (< 1 ppm

oxygen and moisture) and the anode samples were carefully removed from the separator, after which they are rinsed in Dimethyl Carbonate for 10 min under stirring conditions. The samples were then dried under vacuum for 20 min and placed in a sample holder for positron measurements. The sample holder was transported to the PADBS facility in an air-tight box. The positron setup was flushed with N_2 during the placement of the samples, and samples were transferred to the set-up within 1 s, so that minimal contamination with air has occurred. The PADBS setup was brought to vacuum level of 1.10^{-6} mbar after which the positron measurements for 48 different implantation energies have started.

Results and discussion

Figure 6a shows an AFM scan of a pristine flake where the pores are clearly visible. After the scan we added electrolyte to the surface and started the lithiation process for 48 h with a discharge current of 12.5 μA cm^{-2}, after which we removed the electrolyte and performed a new scan. Figure 6b shows the lithiated state of the flake, which confirms the volume absorption by pores and a change of surface as a result of alloying with lithium on the surface.

PADBS results

Ten samples were cycled according to the procedure described above (Fig. 5), using the following values for the total discharged capacity C_d: 50, 150, 250, 350, 700, 1000, 1500, 2000, 2500 and 3000 mAh g^{-1}. We performed PADBS measurements on all samples including a pristine sample which was stored under electrolyte for 48 h and treated the same way as all other samples. Figure 7a, b shows the measured (dots) and fitted (line) S parameter and W parameter as a function of implantation energy for three samples: the pristine sample, and samples with discharge capacities of $C_d = 1000$ mAh g^{-1} and $C_d = 2000$ mAh g^{-1}. The pristine sample shows a relatively flat S-plot and W-plot while the cycled samples show a slope on both S and W parameter between approximately 0–7 keV, which reveals the difference in annihilation characteristics at the surface in comparison to those in the deeper Li affected regions. For higher energies the curve forms a relatively constant S and W which is related to the deeper located bulk material. For this study, we limit ourselves to analyzing the differences in the bulk level of the S and W parameters of energies between 7 and 25 keV (indicated by the vertical gray dashed line in Fig. 7a, b). The dashed arrows in Fig. 7a, b indicate the bulk value of the defect-sensitive S parameter and show significant

Fig. 6 AFM scans of **a** pristine and **b** Highly lithiated flake surface
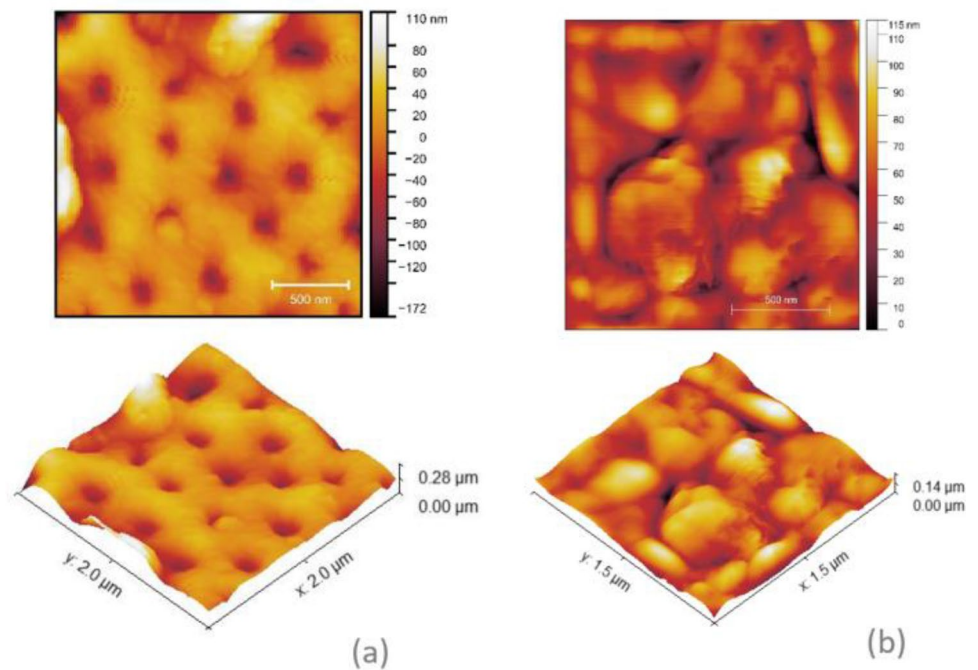
differences between 1000 and 2000 mAh g^{-1}, while the *W* parameter for both samples remains approximately the same.

Figure 7c shows the *S* and *W* parameter in one plot as function of the implantation energy, or equivalently the depth. The characteristic *S*, *W*-point for the bulk for each of the three samples is indicated by the triangles. These bulk level values are used in this study to observe changes in the damage to the material.

In Fig. 8, all samples (with different discharged capacity C_d) are represented by the bulk *S*, *W*-points. With increasing discharge capacity first an increase in the *S* parameter and a decrease in the *W*-parameter is observed. It can be noticed that up to 1000 mAh g^{-1} the bulk *S*, *W*-points lie on a single straight line indicating that the concentration of defects has increased without a noticeable change in defect character, which can be related to structural changes (formation of a-Si) due to the lithium alloying process.

Discharging at 1500 mAh g^{-1} does not lead to further changes in *S* and *W* meaning that defect concentrations are at a level causing positron saturation trapping. However, for higher discharging levels (2000, 2500 and 3000 mAh g^{-1}) a large increase in mainly the *S* parameter is observed, a clear indication for trapping of positron at a different trapping site. The fact that the change in the *W* parameter is less pronounced hints at the formation of larger (crack precursor) defects.

Conclusions

The forming of defects in porous Silicon anodes were investigated for different lithiation conditions by using positron annihilation techniques as a high sensitive defect probe. It appears that the positron energy distribution changes as soon as a new form of defects occurs, so that the origin of the defects can be accurately determined. The method has shown for porous silicon that during the first two cycles, defects are formed above a discharge capacity of 1500 mAh g^{-1}. In general, we conclude that positron techniques appears to be a powerful way to investigate the process of defect development in silicon when used as an anode for Li-ion batteries.

In the study we limited ourselves to the lithiation process and the associated development of defects during the first two cycles of porous silicon anodes. The results found lead to a continuation of this study by looking at the defect development that occurs during long-term cycling and investigation of the influence of discharge and charge rate.

Fig. 7 Low momentum S parameter (**a**) and high momentum W parameter (**b**) and the S–W plot as function of implantation energy (**c**) for a pristine sample, sample $C_d = 1000$ mAh g^{-1} and sample $C_d = 2000$ mAh g^{-1}. An example for determination of the bulk level value is given by the dotted arrows. Bulk S/W points are used for further analysis
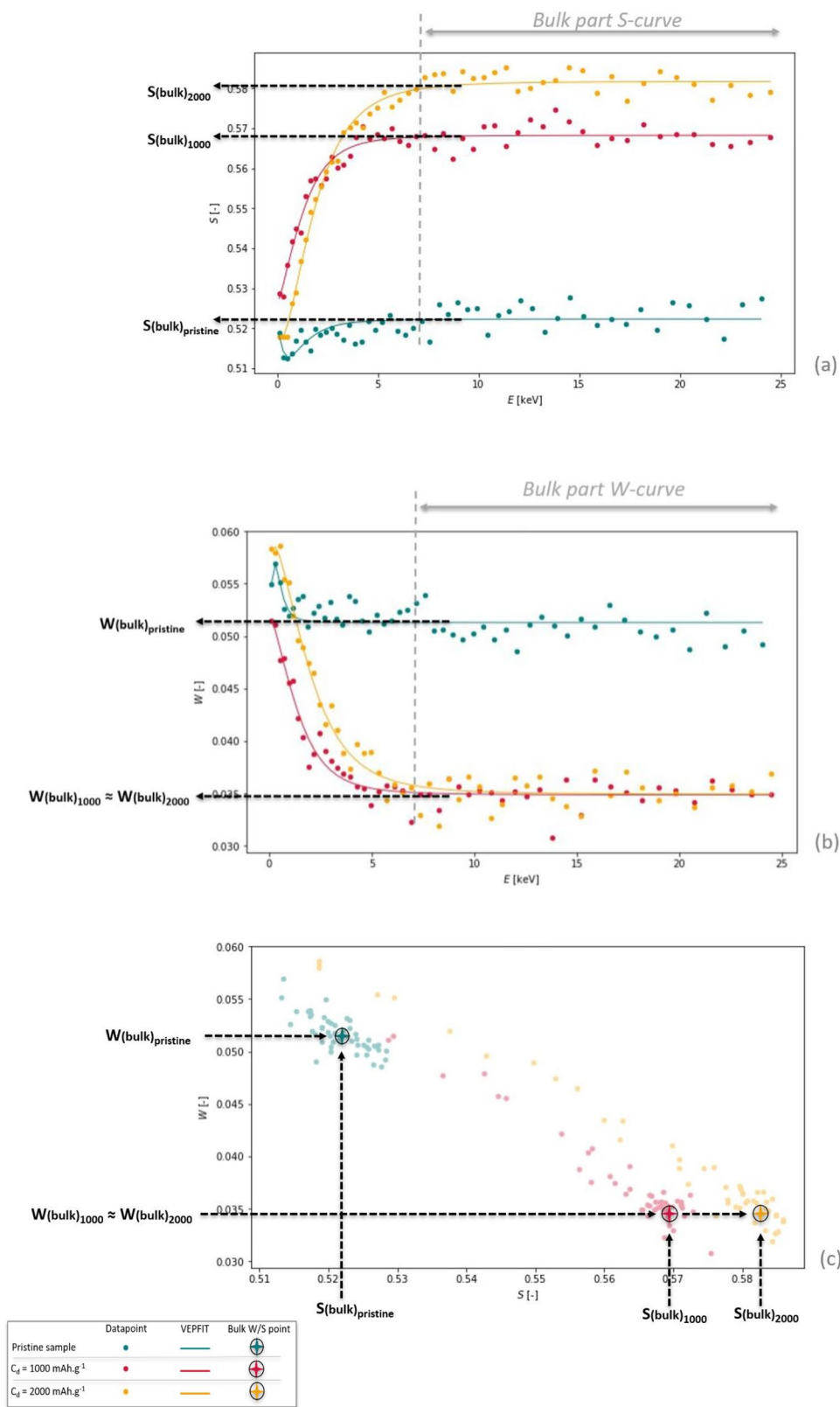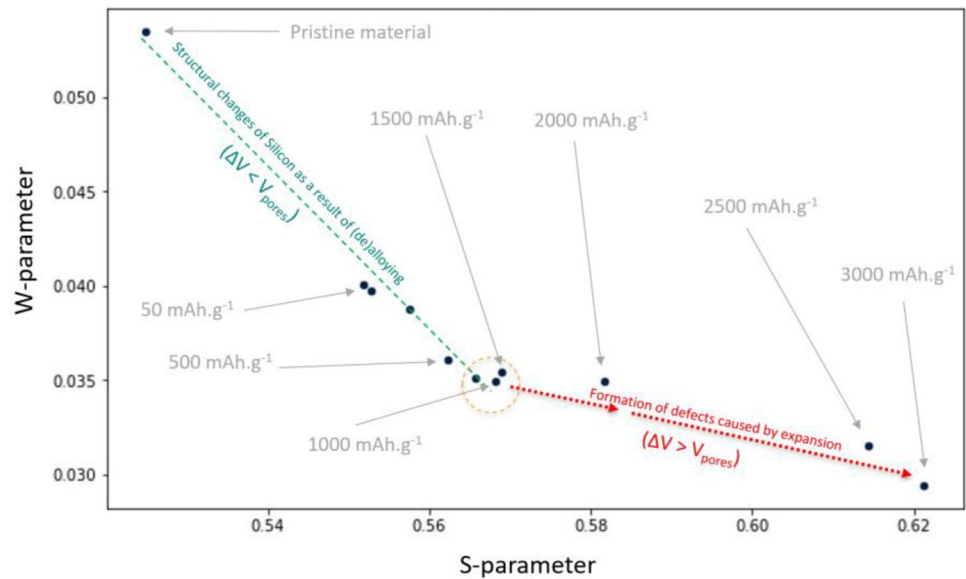
Fig. 8 *S*, *W* plane for bulk (*S*,*W*) values for samples which were cycled against metallic Lithium, discharged to a capacity C_d of respectively 50, 150, 250, 350, 700, 1000, 1500, 2000, 2500 and 3000 mAh g^{-1}) and charged to 1 V vs Li$^+$/Li. Each sample is represented by 1 point

Declarations

References

An W, Gao B, Mei S, Xiang B, Fu J, Wang L et al (2019) Scalable synthesis of ant-nest-like bulk porous silicon for high-performance lithium-ion battery anodes. Nat Commun 10(1):1–11

Beaulieu LY, Eberman KW, Turner RL, Krause LJ, Dahn JR (2001) Colossal reversible volume changes in lithium alloys. Solid-State Lett 4:A137–A140

Cho J (2010) Porous Si anode materials for lithium rechargeable batteries. J Mater Chem 20(20):4009–4014

Chon MJ, Sethuraman VA, McCormick A, Srinivasan V, Guduru PR (2011) Real-time measurement of stress and damage evolution during initial lithiation of crystalline silicon. Phys Rev Lett 107(4):045503

Clement M, De Nijs JMM, Balk P, Schut H, Van Veen A (1996) Analysis of positron beam data by the combined use of the shape-and wing-parameters. J Appl Phys 79(12):9029–9036

Emagy (2020), consulted on 11/4/2021 by https://e-magy.com/product/. Broek op Langedijk

Ge M, Rong J, Fang X, Zhang A, Lu Y, Zhou C (2013) Scalable preparation of porous silicon nanoparticles and their application for lithium-ion battery anodes. Nano Res 6(3):174–181

Huang S, Cheong LZ, Wang S, Wang D, Shen C (2018) In-situ study of surface structure evolution of silicon anodes by electrochemical atomic force microscopy. Appl Surf Sci 452:67–74

Kalnaus S, Rhodes K, Daniel C (2011) A study of lithium ion intercalation induced fracture of silicon particles used as anode material in Li-ion battery. J Power Sources 196(19):8116–8124

Key B, Morcrette M, Tarascon JM, Grey CP (2011) Pair distribution function analysis and solid state NMR studies of silicon electrodes for lithium ion batteries: understanding the (de) lithiation mechanisms. J Am Chem Soc 133(3):503–512

Kim SH, Kim YS, Baek WJ, Heo S, Yun DJ, Han S, Jung H (2018) Nanoscale electrical degradation of silicon–carbon composite anode materials for lithium-ion batteries. ACS Appl Mater Interfaces 10(29):24549–24553

Klinser G, Kren H, Koller S, Würschum R (2019) Operando monitoring of charging-induced defect formation in battery electrodes by positrons. Appl Phys Lett 114(1):013905

Krause-Rehberg R, Leipner HS (1999) Positron annihilation in semiconductors: defect studies, vol 127. Springer, Berlin

Kubota Y, Escaño MCS, Nakanishi H, Kasai H (2007) Crystal and electronic structure of Li 15 Si 4. J Appl Phys 102(5):053704

Legerstee WJ, Boekel M, Boonstra S, Kelder EM (2021) Scanning probe microscopy facility for operando study of redox processes on lithium ion battery electrodes. Front Chem 9

Li J, Dahn JR (2007) An in situ X-ray diffraction study of the reaction of Li with crystalline Si. J Electrochem Soc 154(3):A156–A161

Liu XH, Huang JY (2011) In situ TEM electrochemistry of anode materials in lithium ion batteries. Energy Environ Sci 4(10):3844–3860

Lynn KG, Lutz H (1980) Slow-positron apparatus for surface studies. Rev Sci Instrum 51(7):977–982

McDowell MT, Ryu I, Lee SW, Wang C, Nix WD, Cui Y (2012) Studying the kinetics of crystalline silicon nanoparticle lithiation with in situ transmission electron microscopy. Adv Mater 24(45):6034–6041

McDowell MT, Lee SW, Nix WD, Cui Y (2013) 25th anniversary article: understanding the lithiation of silicon and other alloying anodes for lithium-ion batteries. Adv Mater 25(36):4966–4985

Obrovac MN, Christensen L (2004) Structural changes in silicon anodes during lithium insertion/extraction. Electrochem Solid State Lett 7(5):A93

Ozanam F, Rosso M (2016) Silicon as anode material for Li-ion batteries. Mater Sci Eng B 213:2–11

Rhodes K, Dudney N, Lara-Curzio E, Daniel C (2010) Understanding the degradation of silicon electrodes for lithium-ion batteries using acoustic emission. J Electrochem Soc 157(12):A1354

Salihoglu O, Kahlout YE (2019) Doped silicon nanowires for lithium ion battery anodes. Mater Res 22(2)

Schut H (1990) A variable positron beam facility with applications in materials science. RID TU Delft

Schultz PJ, Lynn KG (1988) Interaction of positron beams with surfaces, thin films, and interfaces. Rev Mod Phys 60(3):701

Seidlmayer S, Buchberger I, Reiner M, Gigl T, Gilles R, Gasteiger HA, Hugenschmidt C (2016) First-cycle defect evolution of Li1−xNi1/3Mn1/3Co1/3O2 lithium ion battery electrodes investigated by positron annihilation spectroscopy. J Power Sources 336:224–230

Shanefield DJ (1991) Tape casting. Concise encyclopedia of advanced ceramic materials. Pergamon, Oxford, pp 469–472

Shen C, Ge M, Luo L, Fang X, Liu Y, Zhang A et al (2016) In situ and ex situ TEM study of lithiation behaviours of porous silicon nanostructures. Sci Rep 6(1):1–11

Shin HC, Corno JA, Gole JL, Liu M (2005) Porous silicon negative electrodes for rechargeable lithium batteries. J Power Sources 139(1–2):314–320

Smedskjaer LC, Manninen M, Fluss MJ (1980) An alternative interpretation of positron annihilation in dislocations. J Phys F Met Phys 10(10):2237

Suzuki K, Barbiellini B, Orikasa Y, Kaprzyk S, Itou M, Yamamoto K et al (2016) Non-destructive measurement of in-operando lithium concentration in batteries via X-ray Compton scattering. J Appl Phys 119(2):025103

Tang J, Yin Q, Wang Q, Li Q, Wang H, Xu Z et al (2019) Two-dimensional porous silicon nanosheets as anode materials for high performance lithium-ion batteries. Nanoscale 11(22):10984–10991

Tuomisto F, Makkonen I (2013) Defect identification in semiconductors with positron annihilation: experiment and theory. Rev Mod Phys 85(4):1583

Van Veen AV, Schut H, Vries JD, Hakvoort RA, Ijpma MR (1991). Analysis of positron profiling data by means of ''VEPFIT''. In: AIP conference proceedings, vol 218, no. 1. American Institute of Physics, pp 171–198

Vidu R, Quinlan FT, Stroeve P (2002) Use of in situ electrochemical atomic force microscopy (EC-AFM) to monitor cathode surface reaction in organic electrolyte. Ind Eng Chem Res 41(25):6546–6554

Wang J, Liao L, Li Y, Zhao J, Shi F, Yan K et al (2018) Shell-protective secondary silicon nanostructures as pressure-resistant high-volumetric-capacity anodes for lithium-ion batteries. Nano Lett 18(11):7060–7065

Wang J, Huang W, Kim YS, Jeong YK, Kim SC, Heo J et al (2020) Scalable synthesis of nanoporous silicon microparticles for highly cyclable lithium-ion batteries. Nano Res 13(6):1558–1563

Yeom SJ, Lee C, Kang S, Wi TU, Lee C, Chae S et al (2019) Native void space for maximum volumetric capacity in silicon-based anodes. Nano Lett 19(12):8793–8800

Zamfir MR, Nguyen HT, Moyen E, Lee YH, Pribat D (2013) Silicon nanowires for Li-based battery anodes: a review. J Mater Chem A 1(34):9566–9586

Zhang WJ (2011) Lithium insertion/extraction mechanism in alloy anodes for lithium-ion batteries. J Power Sources 196(3):877–885

Zhang Z, Wang Y, Ren W, Tan Q, Chen Y, Li H et al (2014) Scalable synthesis of interconnected porous silicon/carbon composites by the rochow reaction as high-performance anodes of lithium ion batteries. Angew Chem 126(20):5265–5269

Publisher's Note Springer Nature remains neutral with regard to jurisdictional claims in published maps and institutional affiliations.